What caused ozone pollution during the 2022 Shanghai lockdown? Insights from ground and satellite observations

Yue Tan and Tao Wang*

Department of Civil and Environmental Engineering, The Hong Kong Polytechnic University, Hong Kong,
5   999077, China

Correspondence to: Tao Wang (tao.wang@polyu.edu.hk)

Abstract. Shanghai, one of China's most important economic centres, imposed a citywide lockdown in April
and May 2022 to contain a resurgence in cases of coronavirus disease 2019. Compared with the 2020
lockdown, the 2022 lockdown occurred in a warm season and lasted much longer, thereby serving as a
10   relevant real-world test of the response of ambient ozone (O_3) concentrations to emission reductions in a
high-O_3 season. In this study, we analysed surface observations of O_3 and nitrogen dioxide (NO_2)
concentrations and satellite-retrieved tropospheric NO_2 and formaldehyde (HCHO) column concentrations
in the first 5 months of 2022 with comparisons to the year 2021. During the 2-month 2022 lockdown, the
maximum daily 8-h average (MDA8) O_3 concentrations at one or more of the city's 19 sites exceeded China's
15   air quality standard of 160 $\mu g/m^3$ 21 times, with the highest value being 200 $\mu g/m^3$. The city-average MDA8
O_3 concentration increased by 28% in April–May 2022 year-on-year, despite sharp declines in NO_2 surface
and column concentrations (both by 49%) and a 19% decrease in the HCHO column concentration. These
results show that the reductions in O_3 precursors and other pollutants during the 2022 lockdown did not
prevent ground-level O_3 pollution. An analysis of meteorological data indicates that there were only small
20   changes in the meteorological conditions and there was little transport of O_3 from the high-O_3 inland regions
during the 2022 lockdown, neither of which can account for the increased and high concentrations of O_3 that
were observed during this period. The mean HCHO/NO_2 ratio in April–May increased from 1.11 in 2021 to
1.68 in 2022, and the correlation between surface O_3 and NO_2 concentrations changed from negative in 2021
to positive in 2022. These results indicate that the high O_3 concentrations in 2022 were mainly due to large

25 reductions in the emissions of NOx and that the decrease in the concentrations of volatile organic compounds
(VOCs) could not overcome the NO titration effect. During the 2022 lockdown, Shanghai's urban centre
remained VOC-sensitive, whereas its semi-rural areas transitioned from VOC-limited to VOC–NOx co-
limited regimes. Our findings suggest that future emission reductions similar to those that occurred during
the lockdown, such as those that will result from electrifying transportation, will not be sufficient to eliminate

30 O_3 pollution in urban areas of Shanghai without the imposition of additional VOC controls or substantial
decreases in NOx emissions.

1 Introduction

Shanghai is a megacity with over 25 million residents and a land area of 6,341 km^2. It serves as a financial,
transport and logistics centre of mainland China. From 27 March to 1 June 2022, the city imposed a strict 2-

35 month lockdown (LCD) to curb increases in the number of cases of coronavirus disease 2019 (COVID-19).
Official statistics indicate that both economic activities and human livelihood were severely disrupted by the
2022 Shanghai LCD (hereinafter '2022 LCD'). For example, in April, year-on-year road passenger traffic
turnover decreased by 85.5% and road cargo turnover decreased by 73.1% (Shanghai Bureau of Statistics,
2022); total industrial output decreased by 61.6% and power generation decreased by 41.7% (National Bureau

40 of Statistics, 2022); and port cargo throughput at the Port of Shanghai, the world's largest seaport, decreased
by 36.5% (Ministry of Transport of the People's Republic of China, 2022). As Shanghai is the most important
transportation and logistics hub of the manufacturing-intensive Yangtze River Delta (YRD) region, the ripple
effects of the LCD in Shanghai have disrupted supply chains of its surrounding provinces, other regions of
China, and the world (Cao et al., 2022; Hale et al., 2022; He, 2022).

45 Such a reduction in human activity can be expected to drastically decrease emissions of air pollutants, as has
been borne out by numerous studies of the 2020 LCD (Wang et al., 2022; Huang et al., 2021; Doumbia et al.,
2021). In this regard, how non-linear chemistry influenced ground-level O_3 concentrations under the chemical
and meteorological conditions of the LCD is of particular interest. Compared with the 2020 LCD in China,

which was imposed in late January–early February, the 2022 LCD in Shanghai was imposed in the high-O_3

50   season and lasted for longer, during which time the O_3 concentrations were higher. In the present study, we

aimed to understand the cause(s) of these higher O_3 concentrations. We first analysed surface observations

of O_3 and NO_2 concentrations and satellite-measured NO_2 and HCHO column concentrations to assess

changes in the concentrations of these species in Shanghai and its surrounding areas during the 2022 LCD.

We then examined the roles of meteorological and chemical conditions in determining O_3 concentrations

55   during the 2022 LCD by analysing small- and large-scale meteorological data and chemical indicators of O_3-

formation regimes. We discuss the implications of our findings for future strategies aimed at reducing O_3

concentrations, which is currently the dominant air pollutant in China in warm seasons.

2 Data and methodology

2.1 Surface measurement data

60   We obtained hourly concentrations of ground-level O_3, NO_2 and particulate matter of 2.5 μm and smaller

($PM_{2.5}$) recorded at ~1,700 stations in China during 2019–2022 from the China National Environmental

Monitoring Centre (http://106.37.208.233:20035/). The national network has 10 stations in Shanghai in 2019-

2020, most of which are situated within the city centre. Since 2021, the number of stations has increased to

20 with most newly added sites locating outside the city centre (refer to Fig. 1 and Fig. S1 for their locations).

65   (Note there were no data from one site (Dianshanhu) in 2021-2022, thus the data from 19 stations are available

for years of 2021 and 2022). The maximum daily 8-h average (MDA8) O_3 concentration was calculated for

each site as the highest value of the 24 8-h moving average O_3 concentrations for a given day. The daily

average concentrations of the other pollutants (NO_2 and $PM_{2.5}$) were also calculated from the hourly data.

The 14-day moving averages of the surface pollutant concentrations were calculated, as these had fewer

70   fluctuations than daily concentrations and thus better revealed trends. Finally, the daily average mixing ratios

of O_x (= O_3 + NO_2) were calculated to account for the titration effect of nitric oxide (NO) on changes in O_3

concentration.

2.2 Satellite and meteorological data

Satellite data were used to investigate the spatiotemporal variations in tropospheric formaldehyde (HCHO)

75   and NO_2 column concentrations during the 2022 LCD period and the same period in 2021. We obtained

Sentinel-5P Level-3 Offline products (HCHO and NO_2) using the TROPOspheric Monitoring Instrument

(TROPOMI) from the Google Earth Engine (GEE; https://earthengine.google.com/) cloud-based platform,

which is an open-source processing system based on JavaScript (Ghasempour et al., 2021). The Sentinel-5P

Level-3 Offline products were converted from the original Sentinel-5P Level-2 Offline data (at a resolution

80   of   5.5   ×   3.5 km)   by   GEE   using   the   harpconvert   tool

(https://cdn.rawgit.com/stcorp/harp/master/doc/html/harpconvert.html) and subjected to a data quality

control process, in which pixels with data quality values less than 75% for NO_2 and less than 50% for HCHO

were removed. Based on the GEE platform, we imported the daily image collections of HCHO and NO_2, cut

them in accordance with the administrative boundary shapefiles of Shanghai (generated from publicly

85   available   geoscience   data   on   the   DataV.GeoAtlas   platform;

http://datav.aliyun.com/portal/school/atlas/area_generator) using a *.clip()* script (Gorelick et al., 2017) and

then averaged the values of all the remaining pixels within the city border to obtain the daily mean

concentrations of HCHO and NO_2. A similar satellite data processing method was used for the YRD region.

We acquired surface site meteorological data (2-m temperature, 2-m relative humidity [RH], 10-m wind

90   direction and 10-m wind speed) from 78 weather stations in Shanghai during April–May in 2021 and 2022,

together with gridded meteorological data (2-m temperature, 1,000-hPa RH, downward ultraviolet (UV)

radiation at the surface, total cloud cover, total precipitation and boundary layer height) from European

Centre   for   Medium-Range   Weather   Forecast   Reanalysis   v5   (ERA5)

(https://cds.climate.copernicus.eu/cdsapp#!/dataset/reanalysis-era5-single-levels   and

95   https://cds.climate.copernicus.eu/cdsapp#!/dataset/reanalysis-era5-pressure-levels). We calculated monthly

averages of the surface-observed meteorological data in 2021 and 2022 and the changes in gridded

meteorological data between 2022 and 2021 to determine the spatiotemporal variations in meteorological conditions in Shanghai and its surrounding regions.

2.3 Backward trajectories analysis

100 The 24-h backward trajectories for Shanghai were calculated at 1-h intervals during April–May 2022 using MeteoInfoMap software (Wang, 2014, 2019) and meteorological data from the Global Data Assimilation System (ftp://arlftp.arlhq.noaa.gov/pub/archives/gdas1/). The endpoints of the trajectories were 500 m above ground level of Shanghai (31.23°N, 121.47°E). Cluster classification was then conducted to divide the trajectories of O_3 exceedance days into five groups based on the origins of air mass.

105 ### 2.4 Site classification and regression analysis

We classified the aforementioned 19 environmental monitoring sites in Shanghai into four types based on land use and mean $HCHO/NO_2$ ratios (Fig. 1 and Fig. 8b). The type A sites (12 sites) are in the city centre (and almost all are within the Shanghai Outer Ring Expressway) and had the lowest $HCHO/NO_2$ ratios; type B are sites in the city perimeter (4 sites) that had moderate $HCHO/NO_2$ ratios; type C are semi-rural sites (2

110 sites) that had the largest $HCHO/NO_2$ ratios; and type D site (one site) is located near the wetland park in the East Chongming Tidal Flat and is least affected by urban emissions but may be influenced by ship emissions. Based on the above classification, we conducted regression analyses between the surface MDA8 O_3 concentrations and daily mean NO_2 concentrations for three types of sites (A, B and C) to examine the O_3 formation regime during the 2022 LCD in Shanghai's city centre, city perimeter and semi-rural sites.

115 ## 3 Results and discussion

3.1 Spatiotemporal variations in surface MDA8 O_3 and NO_2 concentrations

Figure 2 presents the MDA8 O_3 and daily average NO_2 concentrations for the first 5 months of 2021–2022 at the 19 sites in Shanghai. In April–May 2022, the concentrations of NO_2, derived largely from fossil-fuel combustion, decreased by 49% year-on-year, but the average MDA8 O_3 concentrations increased by 12.5%.

120 (In contrast, $PM_{2.5}$ concentrations fell by 30.3% in Shanghai, Fig. S3b). The MDA8 O_3 concentrations

exceeded 160 μg/m³, which is China's Ambient Air Quality Standard for O_3, at one or more of the 19 sites

on 21 days in April–May 2022, with the highest value being 200 g/m³. The average O_x ($O_3 + NO_2$) mixing

ratio in April–May 2022 also increased by 2.2% during the LCD compared with the same period in 2021

(Fig. S3a). These observations indicate that there was significant ground-level O_3 pollution in Shanghai

125 during the 2022 LCD, despite the drastic reductions in human activity. The decrease in NO_2 concentrations

(49%) during the 2022 LCD was larger than the NO_2 decrease during the 2020 LCD (23 January–12 February),

when the average NO_2 concentration decreased by 30.5% from the corresponding period in 2019 (Fig. S2b).

During the 2020 LCD, the average MDA8 O_3 concentrations in Shanghai increased by 13.8% but remained

far below the ambient O_3 concentration standard (Fig. S2a).

130 Figure 3a-c shows the spatial distribution of the MDA8 O_3 concentrations in mainland China and the YRD

region, which consists of Shanghai and three neighbouring provinces (Jiangsu (JS), Anhui (AH) and Zhejiang

(ZJ)), and Shanghai during the 2022 LCD, respectively. It can be seen that elevated O_3 concentrations were

observed in most sites in JS, in the southern part of ZJ and in the eastern part of AH. These provinces are

known to have close economic ties to Shanghai.

135 The increase in MDA8 O_3 concentrations during the 2022 LCD was not restricted to Shanghai. Figure 3d-f

shows the spatial distribution of changes in MDA8 O_3 concentrations from 2021 to 2022 at the national,

regional and city scales, respectively. The MDA8 O_3 concentrations clearly increased in central and eastern

regions but decreased in southwestern, northwestern and northeastern regions (Fig. 3d). The YRD region

recorded one of the greatest increases in MDA8 O_3 concentrations (17.4 μg/m³) during the 2022 LCD (Fig.

140 3e). Within Shanghai, the year-on-year increase in MDA8 O_3 concentrations decreased from urban to semi-

rural areas, with the largest increase recorded in the Putuo district in the city centre (32.9 μg/m³) (Fig. 3f).

3.2 TROPOMI-based HCHO and NO₂ concentrations

Figure 4 depicts the spatial distributions of TROPOMI-based tropospheric column concentrations of HCHO and NO$_2$ and the HCHO/NO$_2$ column ratios in the YRD region. During the 2022 LCD and compared with

145 the same period in 2021, the column concentrations of HCHO, derived from both direct emissions and degradation of anthropogenic and natural volatile organic compounds (VOCs), decreased by 10.8% (Fig. 4a), and the NO$_2$ column concentrations decreased by 25.1% (Fig. 4b). The magnitudes of the reductions in HCHO and NO$_2$ column concentrations had similar spatial distributions, with the largest reductions observed in the region's major cities (Shanghai, Suzhou, Nanjing and Hangzhou). This indicated that the reductions in

150 both the NO$_2$ and HCHO column concentrations were related to decreases in anthropogenic activity during the 2022 LCD. Due to a larger decrease in NO$_2$ concentrations than in HCHO concentrations, the average HCHO/NO$_2$ ratio increased from 2.57 in 2021 to 2.96 in 2022 in the YRD region (Fig. 4c). In Shanghai, the HCHO and NO$_2$ column concentrations decreased by 19.4% and 49.2%, respectively, during the 2022 LCD (see Section 3.3.2 for a detailed discussion). In comparison, the TROPOMI-based HCHO and NO$_2$ column

155 concentrations in February 2020 showed 17% and 38% decreases, respectively, in the YRD region compared with the same month in 2019 (Stavrakou et al., 2021). The much larger reduction in NO$_2$ concentrations than in HCHO concentrations during the 2022 LCD is attributable to the fact that NO$_x$ is mainly emitted by transportation activities (which exhibited the greatest decrease during the 2022 LCD) and by power generation, whereas VOCs are derived from more diverse sources. In Shanghai, the main VOC sources are

160 vehicular exhaust, evaporation of fuels, paints and solvents, petrochemical industries, liquefied petroleum gas and biogenic sources (Lin et al., 2020; Han et al., 2022).

3.3 Cause(s) of high O₃ concentrations during the 2022 LCD

3.3.1 Effects of meteorological conditions on O₃ concentrations in Shanghai

A large body of literature has indicated that meteorological conditions can significantly affect O$_3$

165 concentrations by altering emissions, chemical reaction rates, and distribution and removal processes (e.g.,

Liu and Wang, 2020; Liu et al., 2021). To gain insights into the weather conditions during the 2022 LCD period, we compared several meteorological parameters recorded at surfaces in Shanghai (temperature, RH, and wind speed and direction) (Fig. 5) and the ERA5 reanalysis data for large regions (Fig. 6). The results indicate that during the 2022 LCD, the average surface air temperature and RH decreased compared with the

170   same period in 2021. That is, the mean temperature was 18.4 °C in 2022 versus 19.9 °C in 2021, and the mean RH was 71.4% in 2022 versus 74.2% in 2021 (Fig. 5a-b). The ERA5 reanalysis data revealed there was a decrease in the surface (2-m) temperature in Shanghai, whereas there was an obvious increase in the 2-m temperature in the northern part of the YRD region and a large decrease in the 2-m temperature the southern part of the YRD region (Fig. 6). The decrease in mean temperature in Shanghai during the 2022 LCD may

175   have slowed O_3 production by reducing chemical reaction rates and biogenic emissions. The ERA5 reanalysis data also revealed that during the 2022 LCD there were insignificant changes in cloud cover, downward UV radiation, boundary layer heights and total precipitation in Shanghai but considerable changes in these parameters in the surrounding areas (Fig. 6).

We also assessed whether there was a significant change in surface air flow in Shanghai during the 2022

180   LCD compared with the preceding year. An examination of surface winds in Shanghai showed that during the 2022 LCD, predominant surface winds were from the north–east–southeast sectors (Fig. 5c-d), which is consistent with the 24-h calculated back trajectories (Fig. S4). This indicates that for the majority of the 2022 LCD, Shanghai was upwind of other cities in the YRD region. Compared with the same period in 2021, during the 2022 LCD there was an increase in the occurrence of northerly winds and a decrease in the

185   occurrence of westerly winds. To check for transport of O_3 from high-O_3 areas in the northwest direction, we examined surface wind flows during the 21 O_3-exceedance days. Both surface wind flows and back trajectories indicated that during these days air mainly came from the northeast–east–southeast directions (Fig. 7), indicating that air from other YRD cities contributed little to the high-O_3 days in Shanghai during the 2022 LCD.

190   The above results suggest that the increase in O_3 concentrations in Shanghai during the 2022 LCD were not due to changes in meteorological conditions but were a result of local chemical production.

3.3.2 Effect of the changes in O_3 formation regimes in Shanghai

The photochemical production of O_3 is controlled by the non-linear chemistry of NO_x (NO and NO_2) and VOCs (NRC, 1992). It is well known that in many cities, O_3 concentrations decrease as VOC emissions

195   decrease but increase as NO_x emissions decrease (e.g., Wang et al., 2022). The literature has shown that Shanghai largely operates within a VOC-limited regime (e.g., Lin et al., 2020). We found observational evidence – the $HCHO/NO_2$ ratios and the relationship between O_3 and NO_2 concentrations – that shows that the city remained in a VOC-limited regime before the 2022 LCD (both in the earlier months of 2022 and in April–May of 2021) but may have transitioned near a NO_x-VOC co-limited regime during the 2022 LCD.

200   The $HCHO/NO_2$ ratio has been used as a proxy for O_3 formation regimes, with low ratios indicating VOC-limited conditions, high ratios indicating NO_x-limited conditions, and intermediate values indicating a co-limited regime. Figure 8 shows the temporal variations in city-average $HCHO/NO_2$ ratios in January–May of 2021 and 2022 (Fig. 8a) and the spatial variation of the ratios in Shanghai (Fig. 8b). It indicates that the ratios were comparable (0.56 versus 0.58) in the pre-2022-LCD months of 2021 and 2022 but significantly

205   increased during the 2022 LCD (from 1.11 to 1.68) (Fig. 8a and Fig. S5). Moreover, the ratios were higher in the southern part than the northern part Shanghai, which houses the major urban districts (Fig. 8b).

To determine the regime transition threshold, we adopted an observation-based method similar to that which has been used by previous researchers (Jin et al., 2020; Wang et al., 2021): we plotted the city-average MDA8 O_3 concentrations against the $HCHO/NO_2$ ratio for the first 5 months of 2021 and 2022 (Fig. 9). The peak O_3

210   concentrations increased as the $HCHO/NO_2$ ratio increased and plateaued at approximately 2, indicating that an $HCHO/NO_2$ ratio of 2 was the threshold for transition from a VOC-limited to a co-limited regime. This value is similar to that determined (2.3) for other major Chinese cities (Wang et al., 2021); however, it is less than that determined (~3) for several US cities (Jin et al., 2020) and greater than that which has been derived

(1) from model simulations (Duncan et al., 2010; Li et al., 2021). The city-averaged HCHO/NO$_2$ ratio was greater than 2 on 15 days during the 2022 LCD but on just 2 days in 2021 (see Fig. 9). Moreover, a spatial analysis shows that during the 2022 LCD, the southern part of Shanghai was in a VOC–NOx co-limited regime (with an HCHO/NO$_2$ ratio > 2), whereas the city centre in the northern part remained in the VOC-limited regime (Fig. 8b).

The relationship between surface O$_3$ and NO$_2$ concentrations supports the inference made based on satellite-derived HCHO/NO$_2$ ratio data. It is known that O$_3$ concentrations are negatively correlated with NO$_x$, NO$_y$ or NO$_z$ concentrations (NO$_y$ = NO$_x$ + oxidation products of NO$_x$ [NO$_z$]) under a NO$_x$-titrated condition; this relationship is slightly positive (wug small ΔO$_3$/ΔNO$_x$ ratios) in a VOC-limited regime and very positive (with large ΔO$_3$/ΔNOx ratios) in a NO$_x$-limited regime. For example, previous studies have suggested that an afternoon ΔO$_3$/ΔNO$_z$ ratio (ppb/ppb) less than 4 corresponds to a VOC-limited regime, an afternoon ΔO$_3$/ΔNO$_z$ ratio greater than 7 corresponds to a NO$_x$-limited regime and an afternoon ΔO$_3$/ΔNO$_z$ of 4–7 corresponds to a transition regime (Wang et al., 2017). Only NO$_2$ or NO$_x$ (not other forms reactive nitrogen) are measured by most regular air-monitoring networks, including the China Environmental Monitoring Network used in this study. Figure 10 shows the scatter plot of the MDA8 O$_3$ and daily average NO$_2$ concentrations in three types of sites in Shanghai: the city centre (12 sites), the city perimeter (4 sites) and the semi-rural areas (2 sites). The VOC-limited regime in the city centre sites (with an average HCHO/NO$_2$ ratio of 1.43) had the smallest O$_3$/NO$_2$ slope (3.4) and that in the transition regime sites (with an HCHO/NO$_2$ ratio of 2.27) had the largest O$_3$/NO$_2$ slope (5). In comparison, in 2021, the peak O$_3$ concentration had either a very weak or no correlation with NO$_2$ concentration**s**, indicative of a typical VOC-limited regime. (The type D site had small positive O$_3$/NO$_2$ slopes in both years (0.89-1.17), with high NO$_2$ during the 2022 LCD possibly from the ship emissions in the Yangtze River Estuary, Fig. S6.)

The above results suggest that the increased O$_3$ concentrations observed during the 2022 LCD were mainly due to increased O$_3$ production, which resulted from a larger reduction in NO$_x$ emissions than in VOC emissions under a VOC-limited condition. Additionally, the decrease in particulate emissions, which reduces

the uptake of radicals and O_3 and increases radiation, could have increased O_3 concentrations. Previous model

240   simulations of the 2020 LCD in central China, which saw similar decreases in emissions (i.e., NO_x: ~50%,

PM: ~30%), showed that the decrease in NO_x emissions made a much larger contribution than the decrease

in PM emissions to the increase in O_3 concentrations (Liu et al., 2021). We believe that this also occurred

during the 2022 LCD, i.e., the O_3 concentration increase was mainly due to enhanced O_3 production, which

occurred as a result of a large reduction in NO_x emissions. The O_3 formation regime during the 2022 LCD

245   remained VOC-limited in urban areas but entered co-limiting conditions outside the city centre.

4 Summary and implications

This study analysed the causes of frequent ground-level O_3 pollution during the 2022 LCD (April–May 2022)

in Shanghai and assessed the increases in O_3 concentrations compared with the same periods in previous

years using ground and satellite-based observations. We found that despite large reductions in the activities

250   of transportation sectors and industries during the 2022 LCD, frequent exceedances of the O_3 air quality

standard (~30% days) were observed at ground level. Moreover, the O_3 concentrations were increased during

the 2022 LCD compared with the same period in the preceding year. This increase resulted from a large

reduction in NO_x emissions (~50% from surface and satellite-based measurements) and a small reduction in

VOCs (19% in HCHO column concentrations) within Shanghai. In contrast, meteorology and outside

255   influences had insignificant effects on O_3 concentrations during the 2022 LCD. Moreover, O_3 formation

during the 2022 LCD remained in the VOC-limited regime at most urban and suburban sites but transitioned

to a VOC–NO_x co-limited regime in semi-rural areas.

Our findings on the O_3 response to the 2022 LCD have implications for mitigating summer O_3 pollution,

which has become the predominant air-pollution problem during warm seasons in China. Our results show

260   that decreasing emissions from conventional fossil fuel-powered transportation sectors can lead to increased

O_3 concentrations in VOC-limited urban areas such as Shanghai. China is aiming to have its carbon emissions

peak by 2030 and to achieve carbon neutrality by 2060, which will necessitate the rapid uptake of electric

vehicles in many cities in China. However, although this will greatly improve overall air quality, VOC emissions from other sectors will need to be decreased at the same time to prevent increases in O_3

265 concentrations from the reductions in NO_x (and particulate) emissions in the early stages of phase-out of conventional vehicles. Over time, the wide application and acceptance of renewable energy in transportation and energy production will help cities reach the NO_x-limited formation regime, alleviate ground-level O_3 pollution and achieve carbon-reduction targets.

Code and data availability. The code or data used in this study are available upon request from Tao Wang

270 (tao.wang@polyu.edu.hk).

Supplement. The supplement related to this article is available online at:

Author contributions. TW initiated the research and designed the framework of data analysis. YT processed the data and made the figures. TW and YT analysed the results and wrote the paper.

Competing interests. One author (Tao Wang) is a member of the editorial board of Atmospheric Chemistry

275 and Physics. The peer-review process was guided by an independent editor, and the authors have no other competing interests to declare.

Acknowledgements. This research has been supported by the Hong Kong Research Grants Council (grant no. T24-504/17-N) and the National Natural Science Foundation of China (grant no. 91844301).

References

280 Ministry of Transport of the People's Republic of China: https://www.mot.gov.cn/shuju/, last access: 21 July 2022.

National Bureau of Statistics: https://data.stats.gov.cn/easyquery.htm?cn=E0101, last access: 21 July 2022.

Shanghai Bureau of Statistics: https://tjj.sh.gov.cn/sjfb/index.html, last access: 21 July 2022.

Cao, A., Zhang, S., and Na, E.: Shanghai, home to Tesla, SMIC and GM and Volkswagen's Chinese partner,
is the most important city for China's economy. Here's why, South China Morning Post, 17th May,
2022.

Doumbia, T., Granier, C., Elguindi, N., Bouarar, I., Darras, S., Brasseur, G., Gaubert, B., Liu, Y., Shi, X.,
Stavrakou, T., Tilmes, S., Lacey, F., Deroubaix, A., and Wang, T.: Changes in global air pollutant
emissions during the COVID-19 pandemic: a dataset for atmospheric modeling, Earth System Science
Data, 13, 4191–4206, https://doi.org/10.5194/essd-13-4191-2021, 2021.

Duncan, B. N., Yoshida, Y., Olson, J. R., Sillman, S., Martin, R. V., Lamsal, L., Hu, Y., Pickering, K. E.,
Retscher, C., Allen, D. J., and Crawford, J. H.: Application of OMI observations to a space-based
indicator of NOx and VOC controls on surface ozone formation, Atmospheric Environment, 44, 2213–
2223, https://doi.org/10.1016/j.atmosenv.2010.03.010, 2010.

Ghasempour, F., Sekertekin, A., and Kutoglu, S. H.: Google Earth Engine based spatio-temporal analysis of
air pollutants before and during the first wave COVID-19 outbreak over Turkey via remote sensing,
Journal of Cleaner Production, 319, 128599, https://doi.org/10.1016/j.jclepro.2021.128599, 2021.

Gorelick, N., Hancher, M., Dixon, M., Ilyushchenko, S., Thau, D., and Moore, R.: Google Earth Engine:
Planetary-scale geospatial analysis for everyone, Remote Sensing of Environment, 202, 18–27,
https://doi.org/10.1016/j.rse.2017.06.031, 2017.

Hale, T., Li, G., Dempsey, H., and Olcott, E.: Shanghai Covid lockdown 'will have a global effect on almost
every trade,' Financial Times, 7th April, 2022.

Han, Y., Wang, T., Li, R., Fu, H., Duan, Y., Gao, S., Zhang, L., and Chen, J.: Measurement report:
Simultaneous multi-site observations of VOCs in Shanghai, East China: characteristics, sources and
secondary formation potentials, Atmospheric Chemistry and Physics Discussions, 1–49,
https://doi.org/10.5194/acp-2022-250, 2022.

He, L.: Lockdowns in Shanghai and other Chinese cities pose a growing threat to the economy, CNN Business,
8th April, 2022.

Huang, X., Ding, A., Gao, J., Zheng, B., Zhou, D., Qi, X., Tang, R., Wang, J., Ren, C., Nie, W., Chi, X., Xu,
Z., Chen, L., Li, Y., Che, F., Pang, N., Wang, H., Tong, D., Qin, W., Cheng, W., Liu, W., Fu, Q., Liu,
B., Chai, F., Davis, S. J., Zhang, Q., and He, K.: Enhanced secondary pollution offset reduction of
primary emissions during COVID-19 lockdown in China, National Science Review, 8, nwaa137,
https://doi.org/10.1093/nsr/nwaa137, 2021.

Jin, X., Fiore, A., Boersma, K. F., Smedt, I. D., and Valin, L.: Inferring Changes in Summertime Surface Ozone–NO_x–VOC Chemistry over U.S. Urban Areas from Two Decades of Satellite and Ground-Based Observations, Environ. Sci. Technol., 54, 6518–6529, https://doi.org/10.1021/acs.est.9b07785, 2020.

Li, D., Wang, S., Xue, R., Zhu, J., Zhang, S., Sun, Z., and Zhou, B.: OMI-observed HCHO in Shanghai, China, during 2010–2019 and ozone sensitivity inferred by an improved HCHO ∕ NO_2 ratio, Atmospheric Chemistry and Physics, 21, 15447–15460, https://doi.org/10.5194/acp-21-15447-2021, 2021.

Lin, H., Wang, M., Duan, Y., Fu, Q., Ji, W., Cui, H., Jin, D., Lin, Y., and Hu, K.: O_3 Sensitivity and Contributions of Different NMHC Sources in O_3 Formation at Urban and Suburban Sites in Shanghai, Atmosphere, 11, 295, https://doi.org/10.3390/atmos11030295, 2020.

Liu, Y. and Wang, T.: Worsening urban ozone pollution in China from 2013 to 2017 – Part 1: The complex and varying roles of meteorology, Atmos. Chem. Phys., 20, 6305–6321, https://doi.org/10.5194/acp-20-6305-2020, 2020.

Liu, Y., Wang, T., Stavrakou, T., Elguindi, N., Doumbia, T., Granier, C., Bouarar, I., Gaubert, B., and Brasseur, G. P.: Diverse response of surface ozone to COVID-19 lockdown in China, Science of the Total Environment, 789, https://doi.org/10.1016/j.scitotenv.2021.147739, 2021.

National Research Council: Rethinking the Ozone Problem in Urban and Regional Air Pollution, National Academies Press, 525 pp., 1992.

Stavrakou, T., Müller, J.-F., Bauwens, M., Doumbia, T., Elguindi, N., Darras, S., Granier, C., Smedt, I. D., Lerot, C., Van Roozendael, M., Franco, B., Clarisse, L., Clerbaux, C., Coheur, P.-F., Liu, Y., Wang, T., Shi, X., Gaubert, B., Tilmes, S., and Brasseur, G.: Atmospheric Impacts of COVID-19 on NOx and VOC Levels over China Based on TROPOMI and IASI Satellite Data and Modeling, Atmosphere, 12, 946, https://doi.org/10.3390/atmos12080946, 2021.

Wang, T., Xue, L., Brimblecombe, P., Lam, Y. F., Li, L., and Zhang, L.: Ozone pollution in China: A review of concentrations, meteorological influences, chemical precursors, and effects, Science of The Total Environment, 575, 1582–1596, https://doi.org/10.1016/j.scitotenv.2016.10.081, 2017.

Wang, T., Xue, L., Feng, Z., Dai, J., Zhang, Y., and Tan, Y.: Ground-level ozone pollution in China: a synthesis of recent findings on influencing factors and impacts, Environ. Res. Lett., https://doi.org/10.1088/1748-9326/ac69fe, 2022.

Wang, W., van der A, R., Ding, J., van Weele, M., and Cheng, T.: Spatial and temporal changes of the ozone sensitivity in China based on satellite and ground-based observations, Atmospheric Chemistry and Physics, 21, 7253–7269, https://doi.org/10.5194/acp-21-7253-2021, 2021.

Wang, Y. Q.: MeteoInfo: GIS software for meteorological data visualization and analysis, Meteorological Applications, 21, 360–368, https://doi.org/10.1002/met.1345, 2014.

Wang, Y. Q.: An Open Source Software Suite for Multi-Dimensional Meteorological Data Computation and Visualisation, Journal of Open Research Software, 7, 21, https://doi.org/10.5334/jors.267, 2019.

350
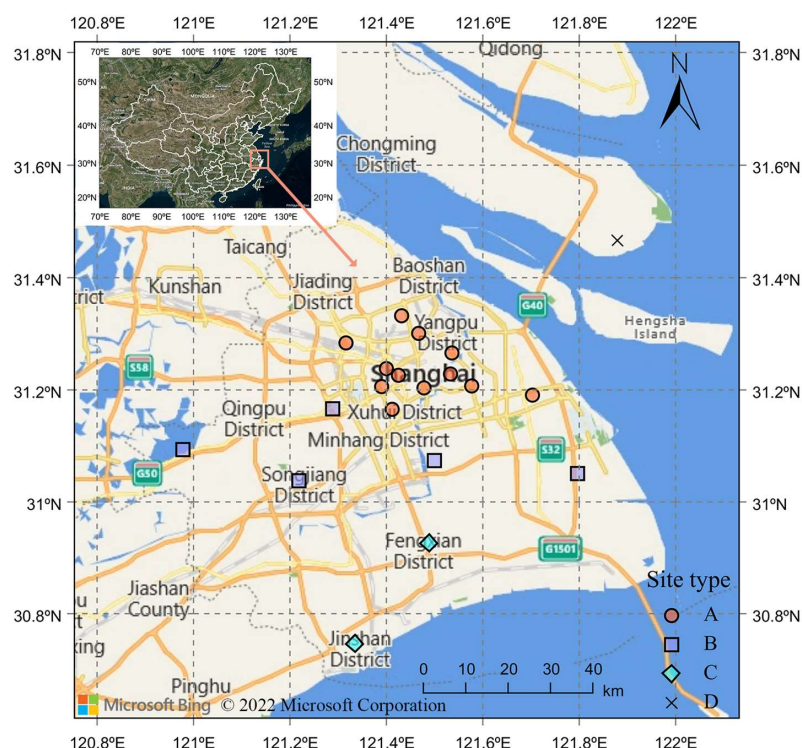
Figure 1. Spatial distribution and classification of the 20 environmental monitoring sites in Shanghai. Types A, B, C and D represent sites in the city centre (12 sites, circles), city perimeter (5 sites, squares), semi-rural area (2 sites, diamonds), and the Yangtze River Estuary (one site, cross), respectively.
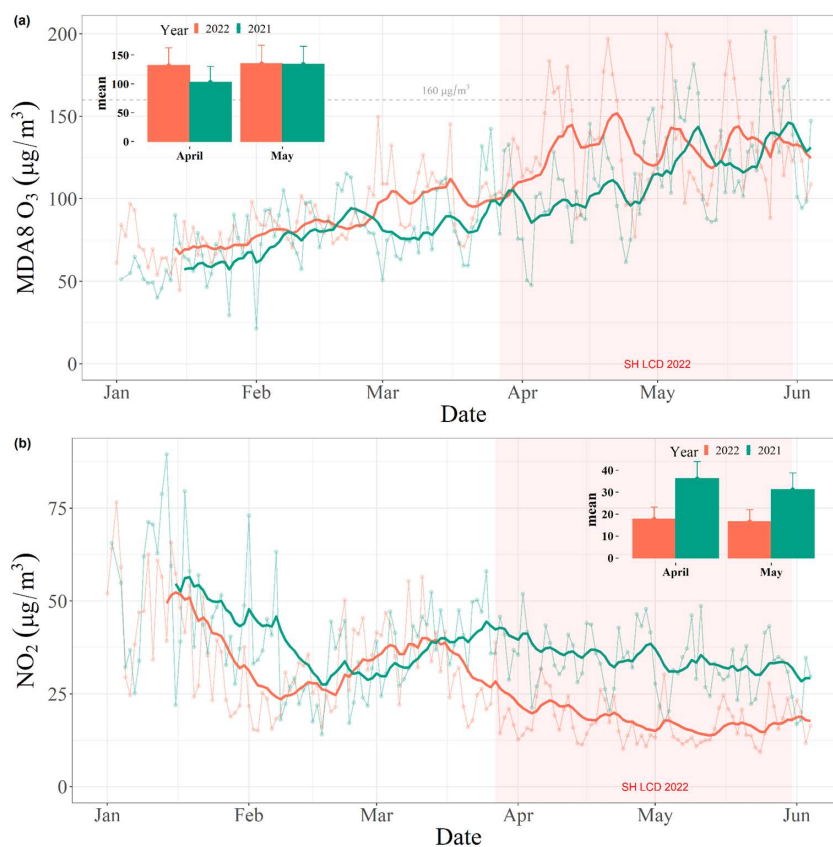
355

Figure 2. Temporal variations in surface-level maximum daily 8-h average (MDA8) O₃ (a) and NO₂ (b) concentrations during the 2022 pre-lockdown (LCD) (1 January to 27 March) and LCD periods (28 March to 31 May) compared with the corresponding periods in 2021. The concentrations are averages from 19 sites in Shanghai. The trend lines represent prior 2-week moving averages. The insert figures show the monthly average concentrations (bars and values indicated by numbers) and standard deviations (error bars). The red background represents the 2022 LCD in Shanghai (SH LCD 2022: 28 March to 31 May). The *x*-axis labels represent the first day of each month.
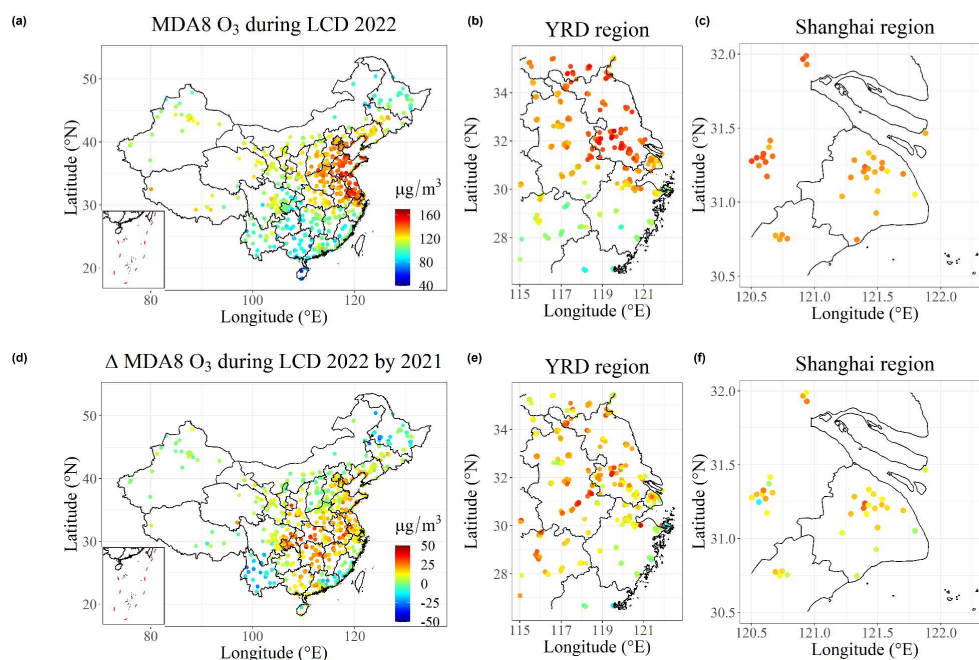
Figure 3. Spatial distribution of surface maximum daily 8-h average (MDA8) O_3 concentrations in 2022 and changes in the same compared with 2021 across all of mainland China (a and d), in the Yangtze River Delta region (b and e) and in Shanghai (c and f) from 28 March to 31 May 2022. LCD: lockdown.
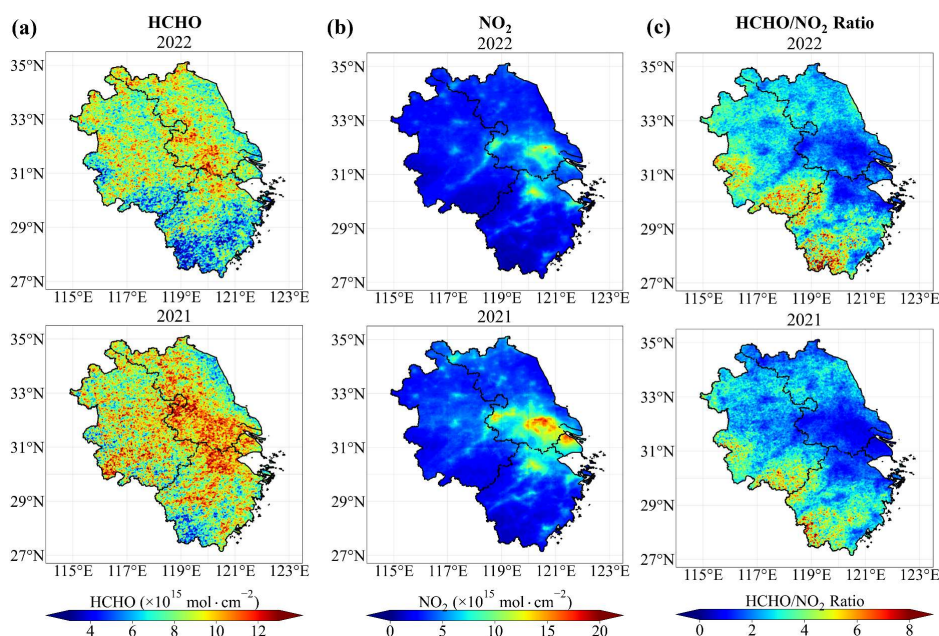
Figure 4. Spatial distribution of the TROPOspheric Monitoring Instrument-based tropospheric column concentrations of HCHO (a) and NO₂ (b) and the HCHO/NO₂ ratio (c) in the Yangtze River Delta region during the 2022 lockdown (upper row) and compared with the same period in 2021 (lower row).
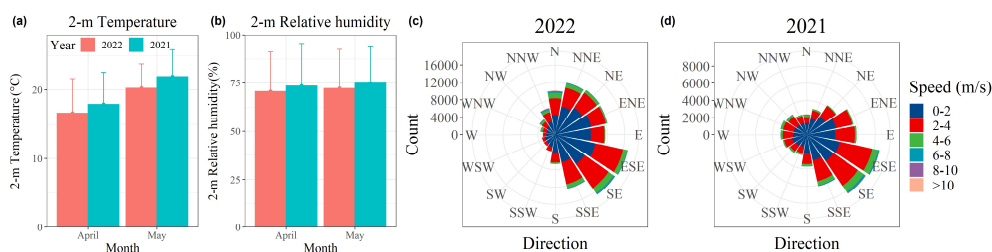
Figure 5. A comparison of average temperature (a) and relative humidity (b) in April and May of 2021 and 2022. Wind rose plots for the 2022 lockdown period (c) and the same period in 2021 (d). The data are surface observations.
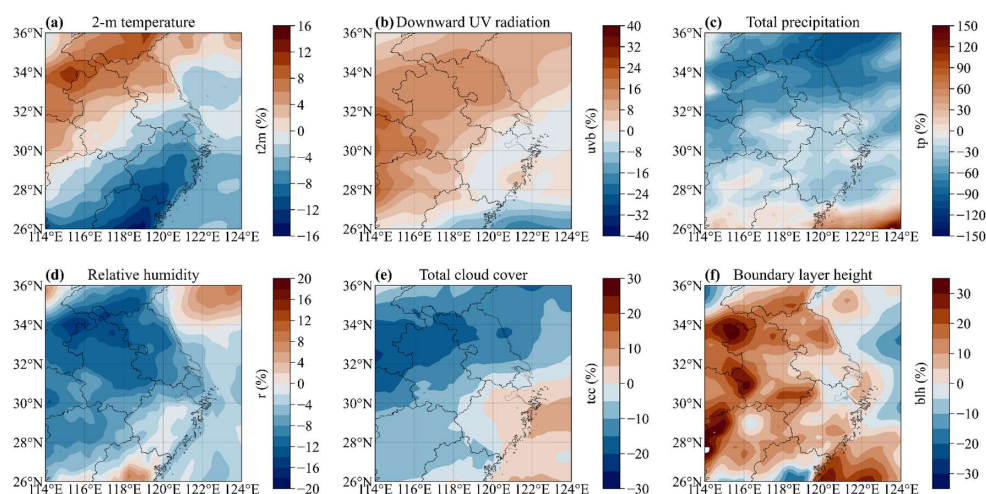
Figure 6. Percentage change in the average meteorological parameters of European Centre for Medium-Range Weather Forecast Reanalysis v5 data for the Yangtze River Delta and its neighbouring regions. 2-m temperature (t2m) (a), downward ultraviolet (UV) radiation at the surface (uvb) (b), total precipitation (tp) (c), relative humidity at 1,000 hPa (r) (d), total cloud cover (tcc) (e) and boundary layer height (blh) (f).
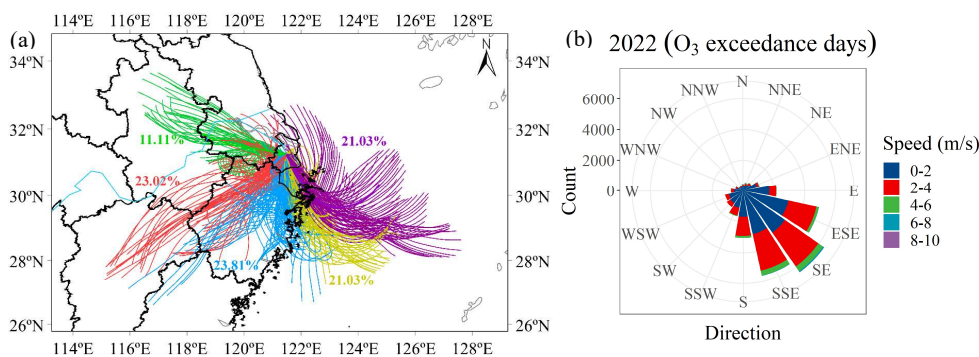
Figure 7. (a) 24-h back trajectories at 1-h intervals at a height of 500 m; and (b) surface wind rose plot for the 21 O_3 exceedance days during the 2022 lockdown in Shanghai. The inserted percentages represent the percentages of trajectory numbers of each classification in the whole trajectories.
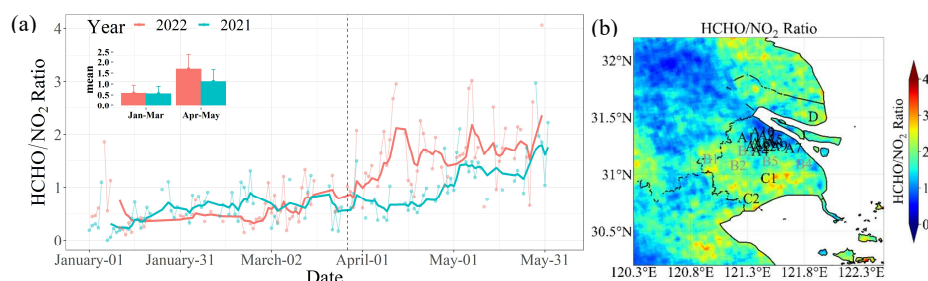
Figure 8. Temporal variations in the city-average HCHO/NO$_2$ ratio from 1 January to 31 May of 2021 and 2022 (a). Spatial variations in the HCHO/NO$_2$ ratio in Shanghai and its surrounding regions during 2022 lockdown (b). The trend lines in (a) represent the moving average by 2 weeks. The red dashed vertical line represents the lockdown starting date (27 March) and the insert shows the monthly average HCHO/NO$_2$ ratios with standard deviations.
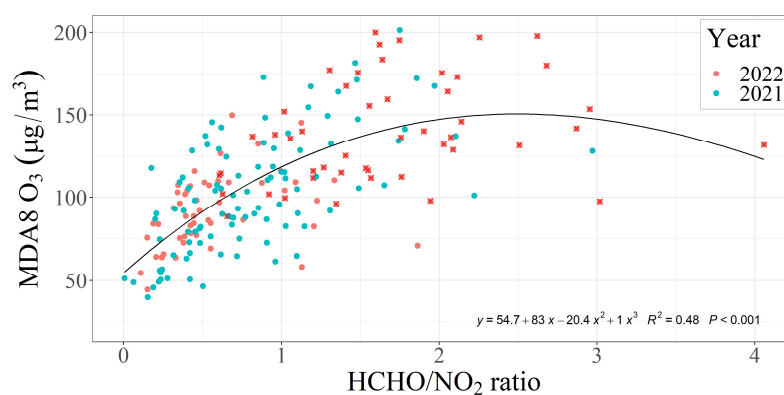
Figure 9. Scatter plot of Shanghai's average maximum daily 8-h (MDA8) O$_3$ concentrations and HCHO/NO$_2$ ratios in January–May of 2021 (blue dots) and 2022 (red dots). The data points recorded during the lockdown periods are labelled with red crosses.
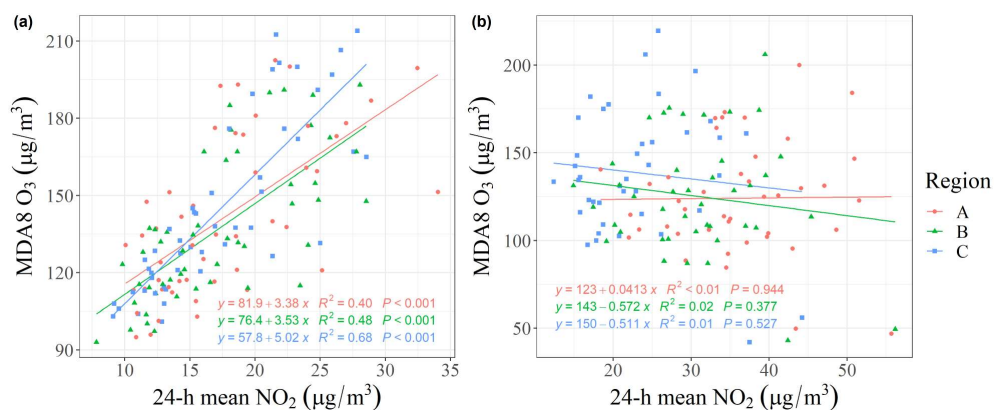
Figure 10. Scatter plots of the surface maximum daily 8-h average (MDA8) O₃ concentrations versus surface daily NO₂ concentrations and their linear regressions (straight lines) during the 2022 lockdown (a) and the same period in 2021 (b) for 3 types of sites.